Solid State Phenomena Vols. 108-109 (2005) pp 1-10 *Online: 2005-12-15*

doi:10.4028/www.scientific.net/SSP.108-109.1

Intrinsic Point Defects in Silicon: a Unified View from Crystal Growth, Wafer Processing and Metal Diffusion

V.V.Voronkov[1,a] and R.Falster[2,b]

[1] MEMC Electoronic Materials, via Nazionale 59, I-39012 Merano BZ, Italy

[2] MEMC Electoronic Materials, viale Gherzi 31, I-28100 Novara, Italy

[a]vvoronkov@memc.it, [b]rfalster@memc.com

Keywords: silicon, vacancy, self-interstitial, zinc, gold, self-diffusion

Abstract. There are several phenomena where the properties of vacancies and self-interstitials in silicon are manifested in straightforward ways. These include the formation of grown-in microdefects, the diffusion of metals (such as Au, Zn), self-diffusion and the installation of vacancy depth profiles in wafers by Rapid Thermal Annealing. Combining features extracted from the analysis of these phenomena, it is possible to define the diffusivities and equilibrium concentrations of the intrinsic point defects. Their diffusivities are remarkably high, and have weak temperature dependence. Their equilibrium concentrations are very low, and have strong temperature dependence.

Introduction

The basic parameters of self-interstitials and vacancies in silicon – the diffusivities D_I and D_V and the equilibrium concentrations C_{Ie} and C_{Ve} – are important in many fields of material science and technology. In spite of numerous efforts, there is still a considerable discrepancy between the parameter values used by different authors. In the present paper, the simplest and most straightforward experimental data relevant to the parameters in question are analyzed. Combining these results, it is possible to reliably determine almost all of the parameters. The main sources of information to analyze are:

- *Crystal growth:* initially incorporated intrinsic point defects give rise to "grown-in" microdefects. Observations of the properties of these microdefects reveal much about the properties of the intrinsic point defects.
- *Metal diffusion into dislocation-free samples:* this process is based on the outward flux of self-interstitials to the sample surface and the inward flux of vacancies from the surface.
- *Self-diffusivity:* measured both under equilibrium and non-equilibrium conditions.
- *Vacancy profile installation into thin wafers:* achieved through Rapid Thermal Annealing (RTA) commercially known as Magic Denuded Zone®.

The parameters of the intrinsic point defects (in their free, unbound states) will be deduced, step by step, while moving through this list.

Grown-in Microdefects in Silicon Crystals

There are two basic types of grown-in microdefects found in dislocation-free silicon crystals. They are voids (formed by agglomeration of vacancies and often referred to as D-defects in the past) and dislocation loops (formed by agglomeration of self-interstitials and often referred to as A-swirl-defects). The microdefect type is normally defined by a simple V/G rule [1,2] where V is the growth rate and G is the axial temperature gradient: voids are formed if V/G somewhat exceeds a certain critical value, while A-swirls are formed if V/G is somewhat below that critical value.

Microdefect Change-over from Interstitial Type to Vacancy Type. The physical reason for the V/G rule is that the type and concentration of intrinsic point defects initially incorporated into a growing crystal, after transient stage of recombination, is controlled [1-3] by the V/G ratio. The critical value of this ratio, for the change-over from self-interstitial incorporation (at lower V/G) to vacancy incorporation (at higher V/G) is expressed through the point defect parameters taken at the melting point (T_m):

$$(V/G)_{cr} = (1/kT_m^2) [P_I (E - \varepsilon_I) - P_V (E - \varepsilon_V)] / (C_{Ve} - C_{Ie}) \quad . \qquad (1)$$

Here P_V is the diffusivity-concentration product for vacancies, $D_V C_{Ve}$, termed the "vacancy transport capacity", and $P_I = D_I C_{Ie}$ is the self-interstitial transport capacity; E is the average of the two formation energies, $(E_I + E_V) / 2$ and ε_V is the drift energy that defines the velocity of the uphill drift of vacancies along the temperature gradient (ε_I is a similar quantity for self-interstitials). The transport capacities are approximately known from metal and self-diffusion [4], the average formation energy is roughly 4 eV, the drift energies are not known definitely but are unlikely to exceed E. The experimental value of $(V/G)_{cr}$ is somewhat uncertain: (0.16 ± 0.04) mm^2/minK [2]. Still, Eq. 1 is useful to estimate the concentration difference $\delta C = C_{Ve} - C_{Ie}$ at the melting point. The resulting value is less than $2x10^{14}$ cm^{-3}.

Void Total Volume. The incorporated vacancy concentration, C_V, is an increasing function of V/G [3] that tends to a saturated value equal to δC. For typical growth conditions, C_V is close to $\delta C/2$. Upon cooling, vacancies are almost completely agglomerated into voids [2]. Experimentally, the total amount of vacancies contained in voids can be obtained from the void density (measured by the Laser Scattering Tomography) and the average volume of voids deduced from the scattering intensity from individual voids [5]. The resulting value for δC is again on the order of $2x10^{14}$ cm^{-3}.

Void Density. If vacancy consumption by a void is diffusion-limited then the predicted dependence of the void density (N_v) on the crystal cooling rate ($q = -dT/dt$) is $q^{3/2}$ [2] – well in accord with reported experimental data [5]. For diffusion-limited void growth, N_v is a sensitive function [2] of the vacancy diffusivity D_V taken at the void nucleation temperature, typically close to 1100°C in Czochralski (CZ) crystals. The value of D_V at 1100°C can be thus deduced using the absolute value of N_v which is around $1.5x10^6$ cm^{-3} at q = 2 K/min. The result is only slightly dependent on the assumed scenario of void production: either by direct nucleation or by an initial nucleation of oxide particles that are subsequently converted into voids by cavitation [6]. The vacancy diffusivity deduced in either scenario is around $5x10^{-5}$ cm^2/s [6,7]. This number implies a very low equilibrium concentration C_{Ve} at 1100°C - about 10^{12} cm^{-3} - using the approximately known [4] transport capacity for vacancies (around $5x10^7$ cm^{-1}s^{-1} at 1100°C). At T_m, the difference $C_{Ve} - C_{Ie}$ is positive; the inequality $C_{Ie} < C_{Ve}$ most likely holds at lower T. Since $P_I > P_V$ at T > 1000°C [4], then $D_I > D_V$ in this temperature range.

Void Striations. In CZ crystals formation of voids is enhanced by oxygen that can be either adsorbed at the void surface (for direct void nucleation) or can aggregate along with vacancies into primary oxide particles (for the cavitation scenario). In both cases the computed void density is insensitive to the oxygen concentration [6,7], in agreement with experiment [8]. In a crystal of strong oxygen striations, however, voids are found to be concentrated in the oxygen-rich layers [8]. This is a clear indication to a high vacancy diffusivity. Voids are formed first in the oxygen-rich layers. The adjacent oxygen-lean layers become quickly depleted of vacancies by diffusion to the voids already existing in the oxygen-rich layers. For such a depletion to suppress void formation, vacancies need to diffuse by a distance comparable to the half-period of the striations (about 1 mm) within a characteristic time of some minutes. This is further evidence that D_V should be as large as the value estimated above.

The general conclusion derived from the microdefect properties is that the equilibrium concentrations of the intrinsic point defects are very low while the diffusivities are high. This notion is strongly supported by the concentration of quenched vacancy species measured in RTA

wafers (to be discussed below). This concentration sets a scale for the equilibrium concentration of vacancies during RTA; it varies from 10^{12} to $2x10^{13}$ cm^{-3} in the range of 1150 to 1280°C [9]. The notion of low concentrations (and corresponding high diffusivities) is of fundamental importance in order to treat properly the metal diffusion data which is the next step of the present analysis.

Metal (Zn, Au) Diffusion

Some metal impurities – zinc, gold, platinum - are dissolved predominantly in substitutional form (M_s) with a small but appreciable interstitial component (M_i). Metal transport occurs by diffusion of the M_i species followed by its conversion into the dominant M_s form by filling vacancies and kicking-out self-interstitials. To produce the M_s species by these reactions, vacancies need to be supplied by diffusion from the surface, and self-interstitials removed by out-diffusion. Given a sufficiently long diffusion time, equilibrium with respect to the two reactions is achieved throughout the sample depth and the concentrations of the metal species C_s and C_i and those of the intrinsic point defects (C_V and C_I) are related by the two mass-action laws:

$$C_i\, C_V / C_s = C_{Ve}\, R_{is} \quad , \qquad C_I\, C_s / C_i = C_{Ie} / R_{is} \quad , \tag{2}$$

where $R_{is} = C_{ie} / C_{se}$ is the ratio of the interstitial and substitutional metal solubilities. There are only two independent variables, for instance C_i and C_s (C_V and C_I are then expressed using Eq. 2).

The two equations for the metal profiles $C_i(z,t)$ and $C_s(z,t)$ can be written considering the total concentration of extra silicon atoms, $C_I - C_V - C_s$, that changes only due to vacancy and self-interstitial diffusion (but is not changed by the reactions) and the total metal concentration, $C_i + C_s$, that changes only due to M_i diffusion:

$$\partial/\partial t[C_s + C_V - C_I] = \partial^2/\partial z^2[D_V C_V - D_I C_I] \quad , \tag{3}$$

$$\partial/\partial t[C_s + C_i] = \partial^2/\partial z^2[D_i C_i] \quad . \tag{4}$$

It is convenient to use the concentrations normalized by the corresponding solubility: $S_s = C_s/C_{se}$, $S_i = C_i/C_{ie}$, $S_I = C_I/C_{Ie}$, $S_V = C_V/C_{Ve}$. In the sample bulk, self-interstitials are present in a supersaturated concentration, $S_I = S_i / S_s$, and vacancies in an undersaturated concentration, $S_V = S_s / S_i$. If the $C_s(z,t)$ profile does not lie too low with respect to the solubility C_{se}, Eq. 3 is greatly simplified by neglecting the concentrations C_V and C_I in the left-hand part. For instance, for gold diffusion at 1098°C, the solubility C_{se} is about $5x10^{16}$ cm^{-3}, while C_{Ve} and C_{Ie} are expected to be about 10^{12} cm^{-3} (or less). For profiles with $C_s/C_{se} > 0.01$, both concentrations C_V and C_I are essentially smaller than C_s. In that case Eqs. 3 and 4, with the variables S_s and S_i, contain only two parameters of the intrinsic point defects: the two transport capacities, P_I and P_V. The other parameters are C_{se}, R_{is} and $P_i = D_i C_{ie}$. The total solubility, $C_e = C_{se} + C_{ie} = C_{se}\,(1 + R_{is})$ is known both for Zn and Au from Neutron Activation Analysis (NAA) of saturated samples [10, 11]. The combination $D^* = P_i/C_e$ is the effective diffusivity measured in heavily dislocated samples [12]. Therefore, we are left with only three fitting parameters: P_I, P_V and R_{is}. Since the R_{is} ratio is small, it has only slight impact on the computed profile $S_s(z,t)$ if S_s is sufficiently high.

Upon normalizing the distance z by the sample thickness d, Eqs. 3 and 4 show that the profiles S_s and S_i evolve in dependence of an effective time, t/d^2. To keep the time unit, the effective time is better defined as $t_{eff} = t\,(d_o/d)^2$, using some arbitrary reference thickness d_o (adopted here to be 500 microns).

The simulations were performed using the general conventional equations for diffusion of the three species (V, I and M_i) with equilibrium boundary conditions at the sample surfaces. Finite rates of the reactions were assumed. The Eqs. 2 to 4 have been used only in discussion of the general features of the diffusion profiles that were then confirmed by the numerical results.

Zinc In-Diffusion. A careful study of Zn in-diffusion was performed at 5 diffusion temperatures:

870, 942, 1021, 1115 and 1208°C [13]. At each T, a series of evolving normalized profiles, $S_s = C_s/C_{se}$ (for several values of the effective time t_{eff}) was monitored by Spreading Resistance Profiling. Since Zn_s is a deep acceptor, only a fraction of Zn_s is charged. For this reason, the absolute value of C_s is of somewhat indefinite reliability, but the normalized concentration S_s is well defined. In the original work [13] the profiles for T > 1000°C were simulated altogether neglecting the vacancy contribution. The profiles at T < 1000°C were simulated under assumption of a very high C_{Ve} which is neither realistic (considering the crystal growth results discussed above) nor consistent with the case of T > 1000°C. A refined simulation is necessary to judge of the values of P_I and P_V.

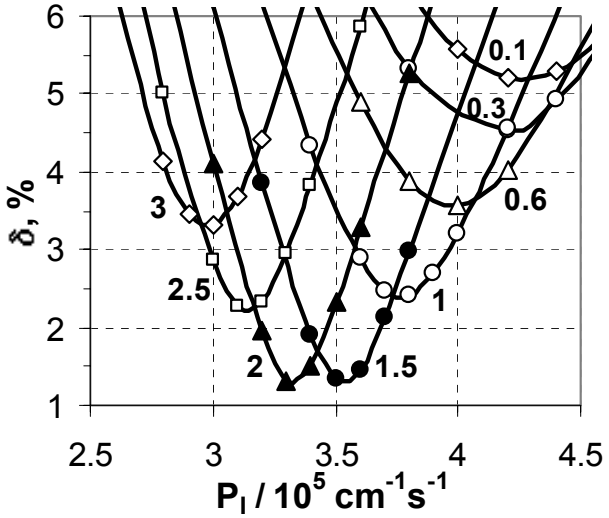

Fig.1 Relative mean square deviation of the computed middle-wafer concentrations of Zn_s from the measured values, plotted in dependence of assumed P_I, for several values of the P_V/P_I ratio (indicated at each curve). The diffusion temperature is 942°C.

The approach used in the present study was to first simulate, at each T, only five profiles of the longest t_{eff}, when the relevant fitting parameters are just P_I and P_V. For several fixed representative values of the P_V/P_I ratio, P_I was varied in a wide range. The criterion of the fit quality was the relative mean square deviation (δ) of the computed middle wafer concentration (C_s/C_{se} at z = d/2) from the measured values, for the selected 5 profiles. An example of computed $\delta(P_I)$ curves is shown in Fig.1, for diffusion at 942°C. A sharp minimum in $\delta(P_I)$ is reached at some value of P_I that depends on the assumed value of P_V/P_I. With the thus-determined best-fit parameters (P_V/P_I = 1.75, P_I = 3.4x10^5 cm^{-1}s^{-1}, in the present example), the profiles of shorter t_{eff} were included into simulation. It turned out that these profiles are sensitive to the R_{is} ratio but not sensitive at all to the assumed diffusivities D_I and D_V - as far as these exceed 5x10^{-6} cm^2/s. At lower values, the fit quality is degraded. This sets a lower limit for D_I and D_V. The estimates based

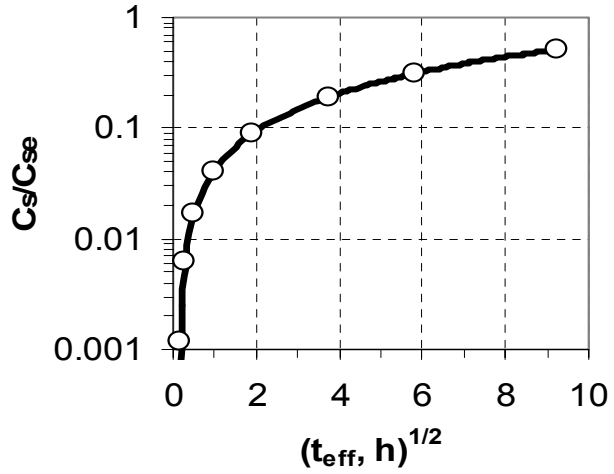

Fig.2 Computed middle-wafer concentration of Zn_s (solid curve) as a function of the effective time, in comparison to the measured values (circles), with the best-fit parameters: P_I = 3.4x10^5 cm^{-1}s^{-1}, P_V/P_I = 1.75 and R_{is} = 0.001 (diffusion at 942°C).

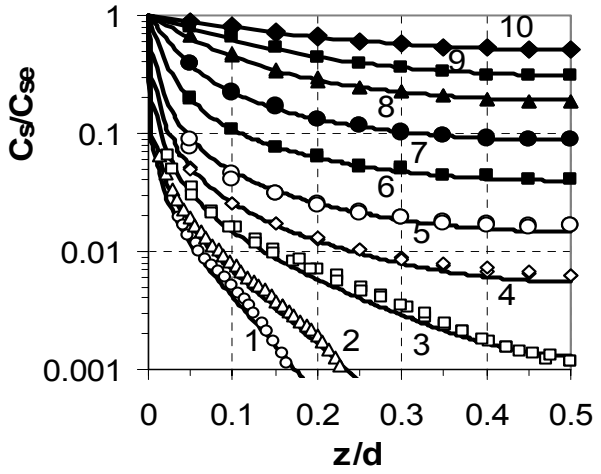

Fig.3 Computed depth profiles of Zn_s (solid curves), in comparison to the measured ones (symbols). The numbers 1 to 10 correspond to increasing effective time t_{eff} at T=942°C, from 15.3 s to 85.6 h. The parameters P_I, P_V/P_V and R_{is} are the same as in Fig.2.

on crystal growth (and also on wafer processing, see below) give essentially higher values, on the order of 10^{-4} cm^2/s.

For the best-fit parameters at 942°C, the computed middle-wafer concentration is shown in dependence of t_{eff} (Fig.2) together with the available measured values (circles) – to illustrate the good quality of the fit. The complete profiles are also well fitted using the same parameters as illustrated in Fig.3. A discussion of the temperature dependence of the best-fit parameters P_I and P_V/P_I is postponed until the gold diffusion profiles are also analyzed.

Gold In-Diffusion. For gold, a series of profiles (for several values of t_{eff}) are available for 3 diffusion temperatures 1000, 1098 and 1200°C [11, 14, 15]. In these studies, the profiles of the total Au concentration ($C = C_s + C_i$) were monitored by NAA and normalized by the total solubility C_e. The data were analyzed [16] in a simplified way: first P_I was deduced using an approximate theoretical expression for the middle-wafer concentration, and then P_V/P_I was deduced by an approximate simulation (assuming a uniform profile for Au_i, neglecting the contribution of Au_i into the total concentration C). All of these assumptions are unnecessary while doing numerical simulations. Accordingly, we have applied a simulation procedure identical to that just used for Zn: the $\delta(P_I)$ dependence is computed for various values of P_V/P_I, to find the best-fit parameters. For gold, all the reported profiles were used to find δ. A peculiarity of this analysis is that a small contribution of Au_i may be important for profiles of the lowest concentration C_s. Therefore, the parameter R_{is} should be also fitted, for every selected combination of P_I and P_V/P_I. The obtained values of R_{is} were always quite small (0.01 or less) and yet a proper choice of R_{is} resulted in some improvement in the averaged deviation δ. A series of the $\delta(P_I)$ curves, for various P_V/P_I, looks similar to those for Zn. An example, for T = 1000°C, is shown in Fig.4. The fit for the middle-wafer concentration as a function of t_{eff} is as good as for the case of Zn (similar to Fig.2). Also the total depth profiles of C/C_e, are well described with the best-fit parameters, similar to Fig.3 for Zn. The only exception is found at T = 1200°C where the profile for the shortest t_{eff} goes too high in the vicinity of the surface. Nevertheless, the middle-wafer concentrations are fitted well for all the profiles.

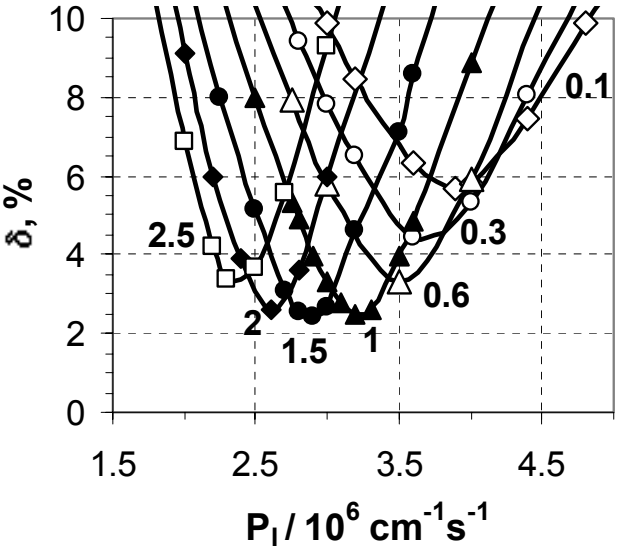

Fig.4 Relative mean square deviation of computed total middle-wafer Au concentrations from the measured values, in dependence of assumed P_I, for several values of P_V/P_I ratio (indicated at each curve). Diffusion at 1000°C.

Temperature Dependence of P_I and P_V/P_I. The best-fit values of P_V/P_I show rather irregular temperature dependence, both for Zn and Au. Therefore, one should allow for some error bar for both parameters P_V/P_I and P_I. The bar is tentatively defined by the condition that the deviation δ is less than 1.5 δ_{min} where δ_{min} is the lowest deviation. For instance, in Fig.1, δ_{min} is 1.3%, and the parameters within the error bar are those leading to δ < 2%. The error bars for the self-interstitial transport capacity P_I are reasonably small (Fig.5); the Zn data are marked by rhombs, and Au data – by circles. This plot is well approximated by an Arrhenius line:

$$P_I = (2.55 \times 10^{26}\ cm^{-1}s^{-1}) \exp(-5.04\ eV / kT) \quad . \qquad (5)$$

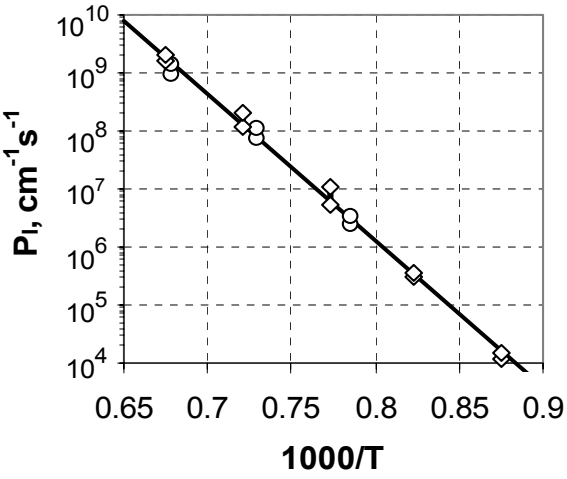

Fig.5 Values of P_I deduced from diffusion of Zn (rhombs) and Au (circles) at different T. The solid line is the best-fit Arrhenius dependence (Eq. 5).

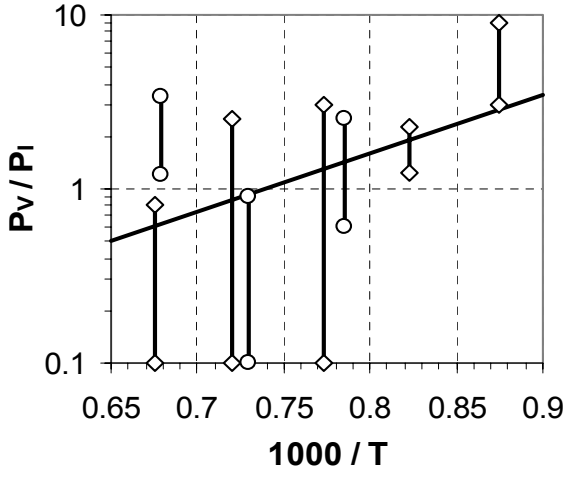

Fig.6 Error bars for P_V/P_I deduced from diffusion of Zn (rhombs) and Au (circles). The solid line is based on the self-diffusion data.

Unfortunately the capacity ratio values show such a strong scatter (Fig.6) that a definite Arrhenius line can not be drawn. The solid line shown in Fig.6 is based on the self-diffusivity results discussed in the next section. The most that can be said is that this line is not inconsistent with the strongly scattered values deduced from metal diffusion.

Self-Diffusion Results

After a long period of contradictory reports, self-diffusivity was at last reliably measured in a wide temperature range using isotope heterostructures [4]. Under equilibrium conditions, the self-diffusivity D_{sd} is a combination of the self-interstitial and vacancy contributions :

$$\rho\, D_{sd} = P_I^* + P_V^* \quad , \tag{6}$$

where ρ is the lattice site density ($5x10^{22}$ cm^{-3}). The quantity P_I^* differs from the transport capacity P_I by a so called correlation factor (f_I) for the tracer jumps: $P_I^* = f_I P_I$. Similarly, $P_V^* = f_V P_V$. The vacancy migrates in a simple way, by jumping to one of the four neighboring sites, and the factor f_V is then equal to 0.5 [17]. For self-interstitials, the path of migration is not definite: it is either via simple jumps into the 4 neighboring interstices or by kicking out one of the 4 lattice neighbors, or a more complicated migration of an interstitialcy (two silicon atoms residing around one lattice site). The value of f_I is therefore not definite.

The measured dependence $D_{sd}(T)$ can be well described by an Arrhenius line with a single activation energy, 4.75 eV [4]. This value is smaller than the activation energy E_{PI} for the self-interstitial component P_I^*, about 5.04 eV by Eq. 5. This shows that there is an appreciable vacancy contribution P_V^* with an activation energy E_{PV} which is smaller than 4.75 eV. A separation of D_{sd} into two components, with a specified E_{PI} (but with the prefactor in P_I^* still to be fitted), is not unique. Almost any value (less than 4.75 eV) can be assumed for E_{PV} with a result of nearly the same averaged deviation of the experimental points from the calculated D_{sd}.

This uncertainty is removed if the data for self-diffusion under oxidation or nitridation conditions [18,19] are invoked. The right-hand part of Eq. 6 is then replaced with $S_I P_I^* + S_V P_V^*$. The supersaturation ratios S_I and S_V were estimated [18] by simultaneous study of diffusion of phosphorus (that migrates predominantly via self-interstitials) and antimony (that migrates predominantly via vacancies). Under oxidation ($S_I > 1$, $S_V < 1$), both the self-diffusion and phosphorus diffusion were enhanced (while antimony diffusion was retarded). Under nitridation

($S_V > 1$, $S_I < 1$), both self-diffusion and antimony diffusion were enhanced (while phosphorus diffusion was retarded). These data were obtained at 1000 and 1100°C, and the implication is that the two components of the self-diffusion, P_I^* and P_V^*, are almost identical in this temperature range. With this constraint, the acceptable values for the activation energy E_{PV} of the vacancy contribution are now limited to a narrow range 4.3 to 4.5 eV. With the deduced P_I^* and known P_I, the correlation factor $f_I = P_I^*/P_I$ is derived to be 0.5 to 0.6 (depending on the assumed E_{PV}).

It turns out (next section) that the RTA profiles of vacancies are more consistent with the higher value of E_{PV}. With E_{PV} = 4.5 eV and E_{PI} = 5.04 eV, the deduced vacancy contribution P_V^* is used to specify the vacancy transport capacity, $P_V = P_V^* / f_V$:

$$P_V = (2.4\text{x}10^{24}\ \text{cm}^{-1}\text{s}^{-1})\ \exp(-4.5\ \text{eV} / kT) \quad . \tag{7}$$

The capacity ratio, according to Eqs. 5 and 7, is shown in Fig.6 by the solid line.

Vacancy Profiles in RTA Wafers

Rapid Thermal Annealing (RTA) at T > 1150°C was shown to saturate the wafers with vacancies and self-interstitials already after several seconds [20], which is consistent with the notion of high diffusivity of the intrinsic point defects. Upon a subsequent quench, vacancies survive in the sample bulk while the near-surface region becomes depleted of vacancies due to out-diffusion. This effect is particularly manifested in the depth profiles of subsequently formed oxide precipitates since oxygen precipitation is strongly enhanced in the presence of these vacancies: there is a wide precipitate-free near-surface region termed the Magic Denuded Zone (MDZ®) [20].

In creating the MDZ® effect, it is important that the free vacancies V can be trapped by oxygen to form VO and VO_2 [9, 21]. For oxygen concentrations typical of CZ silicon, free vacancies dominate above some characteristic binding temperature T_b estimated to be around 1050°C [21]; at T < T_b, the dominant state is VO_2. Therefore, efficient vacancy out-diffusion is limited to the temperature interval from T_{RTA} to T_b. The quenched–in vacancies exist mostly in the form of VO_2, and the concentration of VO_2 can be measured by diffusion of Pt or Au at around 730°C. At this temperature, the transport capacities P_I and P_V are quite low, and the substitutional metal M_s is created in the sample bulk only by filling the existing vacancy species: $M_i + VO_2 \rightarrow M_s + O_2$. Since the metal solubility C_{se} well exceeds the equilibrium concentration of VO_2 (for specified oxygen concentration), almost all vacancy species

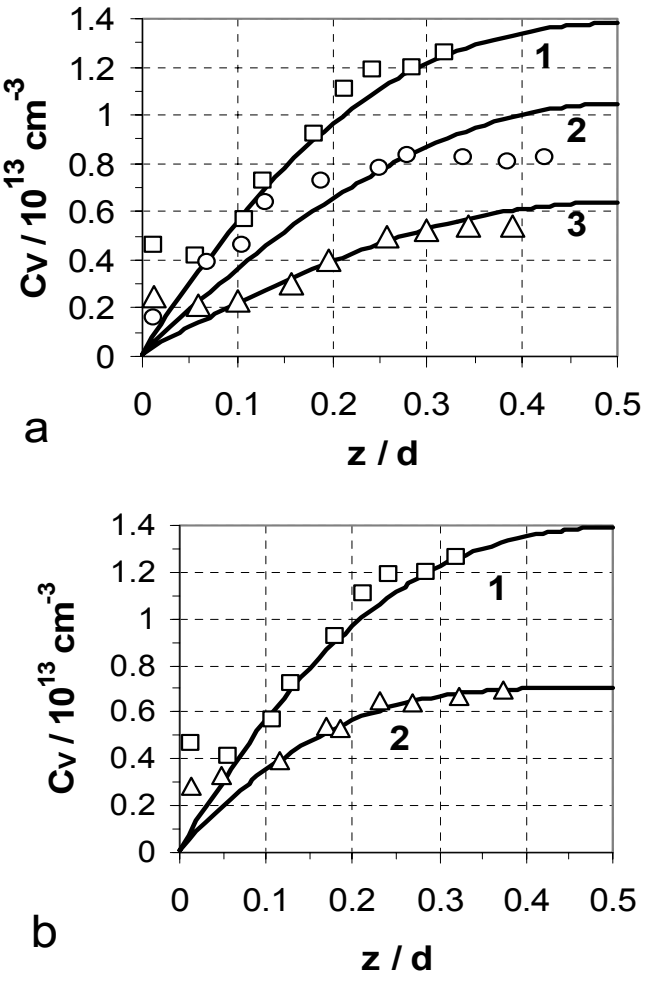

Fig.7 Computed depth profiles of quenched-in vacancy species (solid curves) and the profiles monitored by Au diffusion (symbols), after RTA at 1240°C. (a): three different cooling rates, 100, 40 and 20 K/s for the curves 1, 2 and 3 (same RTA time of 10 s); (b) two different times of RTA, 10 and 2 s for the curves 1 and 2 (same cooling rate of 100 K/s).

are converted into M_s. The depth profile of M_s is measured by DLTS, and thus the vacancy depth profile is obtained. Another way to judge of the vacancy depth profile is to induce oxygen precipitates (e.g. by annealing 800 + 1000°C) and to monitor the precipitate density $N_p(z)$. However, the translation of N_p into the vacancy concentration is not unambiguous since the measured density N_p is often scattered significantly.

In the present study, the RTA processing was done at 1240°C for 10s, with different characteristic cooling rates, 100, 40 and 20 K/s (with known actual temperature profiles T(t)). It is the dependence of the profile shape on the cooling rate that gives most important information on the vacancy diffusivity. One wafer was subjected to a shorter RTA (2 s) with subsequent fast quench (100 K/s). The dependence of the vacancy profile on the RTA duration is also a valuable source of information. The vacancy depth profiles were monitored by Au diffusion at 730°C for 3 h (the diffusion/DLTS test was performed by Prof. E.Yakimov to whom the present authors are grateful).

The $C_V(z)$ and $C_I(z)$ profiles developed in a wafer after a full cycle (ramp-up to T_{RTA}, holding at T_{RTA} and ramp-down) are controlled by diffusion and recombination. The net recombination rate is $K (C_I C_V - C_{Ie} C_{Ve})$. The value of the recombination coefficient K at T_{RTA} is not known. The simulations were performed assuming various representative values of K.

For $K < 10^{-14}$ cm^3/s the recombination is negligible in the time scale of ramp-down. Then the self-interstitials (faster diffusers) almost completely out-diffuse from the wafer. The frozen-in vacancy concentration (for the fastest quench, in the middle of wafer) is close to the initial value of C_{Ve}.

For $K > 10^{-12}$ cm^3/s the recombination is almost instantaneous thus supporting $C_I C_V$ product at the equilibrium value of $C_{Ie}C_{Ve}$. In this case the self-interstitials are almost completely annihilated by the vacancies. The frozen-in vacancy concentration (for the fastest quench, in the middle of wafer) is close to the initial difference $C_{Ve} - C_{Ie}$.

Since the capacities, $P_I = D_I C_{Ie}$ and $P_V = D_V C_{Ve}$, are already specified, there are basically only two fitting parameters: C_{Ie}, C_{Ve} (or D_I, D_V), for every assumed K. Fortunately, the best-fit vacancy diffusivity (at T_{RTA}) was found to be only slightly sensitive to K, and quite a definite value for D_V is deduced, (1 to 1.7)x10^{-4} cm^2/s. The best-fit value of D_I is less definite although always is significantly higher than D_V. A reasonably good fit to both the 3 profiles of different cooling rates, and the 2 profiles of different RTA duration is achieved only under assumption of small K. The best-fit computed profiles for slow recombination ($K = 3x10^{-15}$ cm^3/s) are compared to the measured ones in Fig.7. These profiles correspond to $D_V = 1.7x10^{-4}$ cm^2/s and $D_I = 7x10^{-4}$ cm^2/s (and $C_{Ve} = 1.5x10^{13}$ cm^{-3}, $C_{Ie} = 6x10^{12}$ cm^{-3}).

It should be noted, at this point, that the used value of K means "slow recombination" only regarding very fast cooling in the RTA. Regarding the crystal growth (defect incorporation at T close to T_m) this value of K still means very fast recombination that maintains the $C_I C_V$ product at the equilibrium value.

Temperature Dependence of Diffusivities and Equilibrium Concentrations

Thus far we have two independent estimates for D_V at high T: $5x10^{-5}$ cm^2/s at 1100°C (that comes from void density in crystal growth) and $\approx 1.5x10^{-4}$ cm^2/s at 1240°C (that comes from the above-discussed vacancy profiles in RTA wafers). At very low T, the trapping time of radiation-induced vacancies by oxygen was reported [22]. If diffusion-limited, the trapping time is $1/(4 \pi r D_V C_{ox})$ where C_{ox} is the oxygen concentration and r is the capture radius (a conventional value for r is

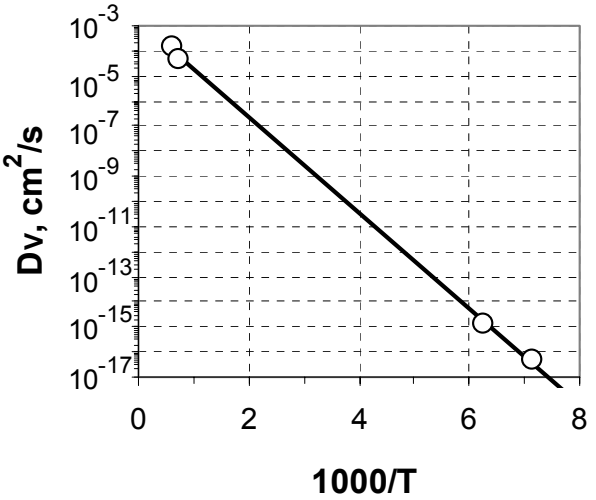

Fig.8 Vacancy diffusivity at high and low T. The solid curve is the Arrehnius line by Eq. 8.

$5x10^{-8}$ cm). The deduced values for D_V are shown, together with the two high-T values, in Fig.8. It is remarkable that the points correspond reasonably well to a single activation (migration) energy of about 0.38 eV. The prefactor in D_V is not quite certain due to some difference between the two high-T points. Yet the $D_V(T)$ function can now be specified in a reasonably definite way:

$$D_V = (0.002\ cm^2/s)\ exp(-0.38\ eV\ /kT) \quad , \tag{8}$$

with an uncertainty in the prefactor of about 30%. The equilibrium concentration, C_{Ve}, is next specified as P_V/D_V:

$$C_{Ve} = (1.2x10^{27}\ cm^{-3})\ exp(-4.12\ eV\ /\ kT) \quad . \tag{9}$$

At T_m, the concentration difference $C_{Ve} - C_{Ie}$ is about $1.5x10^{14}$ cm^{-3}, for Eq. 1 to be consistent with the experimental values for $(V/G)_{cr}$, with now specified transport capacities P_I and P_V. Thus C_{Ie} is expressed through this difference and C_{Ve}. Then D_I at T_m is found as P_I/C_{Ie}. The parameters at T_m – which are especially important for the incorporation stage of the intrinsic point defects during crystal growth – are collected in the Table 1. These are the average numbers, and one should allow for an uncertainty which is roughly 30% for D_V, C_{Ve} and 40% for D_I, C_{Ie}. For the transport capacities, the uncertainty is thought to be much smaller.

Table 1 Parameters at T_m

Quantity	Value
P_I	$2.2x10^{11}$ [$cm^{-1}s^{-1}$]
P_V	$8.6x10^{10}$ [$cm^{-1}s^{-1}$]
D_I	$5.1x10^{-4}$ [cm^2/s]
D_V	$1.5x10^{-4}$ [cm^2/s]
C_{Ie}	$4.4x10^{14}$ [cm^{-3}]
C_{Ve}	$5.9x10^{14}$ [cm^{-3}]

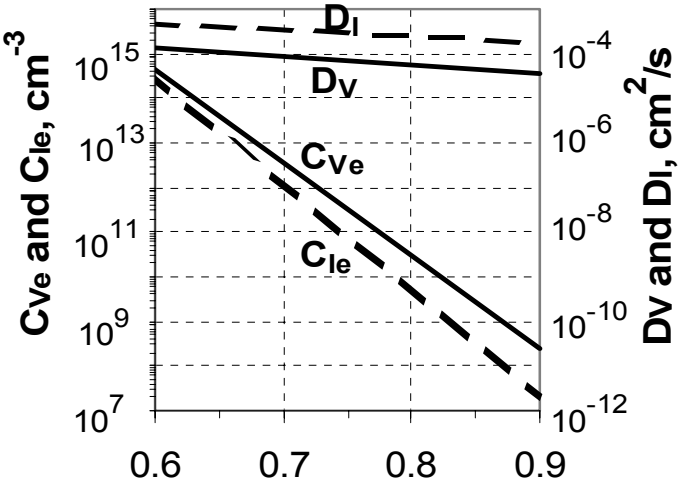

Fig.9 Temperature dependence of the diffusivities D_V and D_I (right axis) and the equilibrium concentrations C_{Ve} and C_{Ie} (left axis) derived in the present work.

The only remaining parameter not yet defined is the migration energy of self-interstitials, E_{Im}. Since a high value of D_I at 1240°C - comparable to $D_I(T_m)$ - follows from simulations of the vacancy profiles in the previous section, we can conclude that E_{Im} is relatively small, most likely less than 0.4 eV. A more definite number is difficult to define since the temperature of 1240°C is too close to T_m. For the sake of completeness we tentatively adopt E_{Im} = 0.3 eV. With this (still somewhat questionable) number we can specify the $D_I(T)$ and $C_{Ie}(T)$ functions :

$$D_I = (0.004\ cm^2/s)\ exp(-0.3\ /\ kT), \tag{10}$$

$$C_{Ie} = (6.4x10^{28}\ cm^{-3})\ exp(-4.74\ eV/kT). \tag{11}$$

The temperature dependence of the equilibrium concentrations and the diffusivities is shown in Fig.9 (the temperature range is approximately from 1390 down to 840°C).

Summary

Combining the experimental data from various fields – crystal growth, metal and self- diffusion, wafer processing by RTA, low-temperature irradiation – it is possible to define almost all the parameters of the intrinsic point defects in silicon. First, the transport capacity of self-interstitials

($P_I = D_I C_{Ie}$) is deduced from metal diffusion data, essentially using a concept of very low equilibrium concentrations of both vacancies and self-interstitials that follows from crystal growth data. Next, also the transport capacity of vacancies ($P_V = D_V C_{Ve}$) is extracted from the self-diffusion data. Finally the vacancy diffusivity D_V at high T is deduced using data on void density and on vacancy profiles in RTA wafers while D_V at very low T is deduced from the irradiation experiments. The $D_V(T)$ function is thus defined. Finally, the vacancy equilibrium concentration C_{Ve} is specified as P_V/D_V. While the vacancy parameters are well defined, the splitting of P_I into D_I and C_{Ie} is not yet quite certain; only at T_m such a splitting can be done.

An additional source of information on the defect parameters is provided by the microdefect patterns observed in crystals grown under varying V/G and composed of vacancy-type bands and self-interstitial-type bands [23-25]. The main difficulty of this approach is that a large number of parameters should be fitted simultaneously. With most of the parameters already specified in the present study, the fitting task may become much simpler. In particular, it may be hoped that an analysis of the microdefect patterns could lead to a more definite value for the self-interstitial migration energy.

References

[1] V.V.Voronkov: J. Crystal Growth Vol. 59 (1982), p. 625.
[2] V.V.Voronkov and R.Falster: J. Crystal Growth Vol. 194 (1998), p. 76.
[3] V.V.Voronkov and R.Falster: J. Appl. Physics Vol. 86 (1999), p. 5975.
[4] H.Bracht, E.E.Haller and R.Clark-Felps: Phys. Rev. Letters Vol. 81 (1998), p.393.
[5] T.Saishoji, K.Nakamura, N.Nakajima, T.Yokoyama, F.Ishikawa and J.Tomioka: High Purity Silicon Vol. 98-13 (1998), p.28.
[6] V.V.Voronkov: Materials Science and Engineering Vol. B56 (1999), p.69.
[7] V.V.Voronkov and R.Falster: J. Crystal Growth Vol. 273 (2005), p. 412.
[8] K.Nakamura, T.Saishoji and J.Tomioka: High Purity Silicon Vol. PV2004-5 (2004), p.237.
[9] R.Falster, V.V.Voronkov and F.Quast: Phys. Stat. Sol. Vol. B222 (2000), p.219.
[10] D.Grunebaum, Th.Czekalla, N.A.Stolwijk, H.Mehrer, I.Yonenaga and K.Sumino: Appl. Phys. Vol. A53 (1991), p.65.
[11] N.A.Stolwijk, B.Schuster, J.Holzl, H.Mehrer and W.Frank: Physica Vol. 116B (1983), p.335.
[12] H.Bracht and H.Overhof: Phys. Stat. Sol. Vol.A158 (1996), p.47.
[13] H.Bracht, N.A.Stolwijk and H.Mehrer: Phys. Rev. Vol. B52 (1995), p.16542.
[14] N.A.Stolwijk, B.Schuster and J.Holzl: Appl. Phys. Vol. A33 (1984), p.133.
[15] J.Hauber, N.A.Stolwijk, L.Tapfer, H.Mehrer and W.Frank: J. Phys. C: Solid State Phys. Vol. 19 (1986) p.5817.
[16] F.Morehead, N.A.Stolwijk, W.Meyberg and U.Gosele: Appl. Phys. Letters Vol. 42 (1983), p.690.
[17] K.Compaan and Y.Haven: Trans. Faraday Soc. Vol. 52 (1956), p.786.
[18] A.Ural, P.B.Griffin and J.D.Plummer: Appl. Phys. Letters Vol. 73 (1998), p.1706.
[19] A.Ural, P.B.Griffin and J.D.Plummer: Phys. Rev. Letters Vol. 83 (1999), p.3454.
[20] R.Falster, M.Pagani, D.Gambaro, M.Cornara, M.Olmo, G.Ferrero, P.Pichler and M.Jacob: Solid State Phenomena Vol.57-58 (1997), p.129.
[21] V.V.Voronkov and R.Falster: J. Electrochem. Soc. Vol. 149 (2002), p. G167.
[22] G.D.Watkins: J. Phys. Soc. Japan Vol. 18 Suppl. II (1963), p.22.
[23] T.Sinno, R.A.Brown, E.Dornberger and W.von Ammon: J. Electrochem. Soc. Vol.145 (1998), p.303.
[24] K.Nakamura, T.Saishoji and J.Tomioka: Semiconductor Silicon Vol.2002- 2 (2002), p.554.
[25] V.V.Voronkov and R.Falster: High Purity Silicon Vol. PV2002-20 (2002), p.16.

Gettering and Defect Engineering in Semiconductor Technology XI
10.4028/www.scientific.net/SSP.108-109

Intrinsic Point Defects in Silicon: a Unified View from Crystal Growth, Wafer Processing and Metal Diffusion
10.4028/www.scientific.net/SSP.108-109.1